

# Rippling Ferroic Phase Transition and Domain Switching In 2D Materials

Yang Yang, Hongxiang Zong,\* Jun Sun, and Xiangdong Ding\*

Ripples are a class of native structural defects widely existing in 2D materials. They originate from the out-of-plane flexibility of 2D materials introducing spatially evolving electronic structure and friction behavior. However, the effect of ripples on 2D ferroics has not been reported. Here a molecular dynamics study of the effect of ripples on the temperature-induced ferroic phase transition and stress-induced ferroic domain switching in ferroelastic-ferroelectric monolayer GeSe is presented. Ripples stabilize the short-range ferroic orders in the high-temperature phase with stronger ferroicity and longer lifetime, thereby increasing the transition temperature upon cooling. In addition, ripples significantly affect the domain switching upon loading, changing it from a highly correlated process into a ripple-driven localized one where ripples act as source of dynamical random stress. These results reveal the fundamental role of ripples on 2D ferroicity and provide theoretical guidance for ripple engineering of controlled phase transition and domain switching with potential applications in flexible 2D electronics.

are currently inaccessible.<sup>[5,6]</sup> Induced inhomogeneous strain also enables the concept proposal and experimental realization of exciton funnel.<sup>[7–9]</sup> Remarkably, the flexural mode also leads to the formation of ripples,<sup>[10]</sup> a class of intrinsic structural defects in 2D materials. Atomistically, ripples are quantized, referred to as ripplocations, and the ripplocations carrying the same sign exhibit an intriguing attractive behavior which is in direct contrast to the well-known repulsive behavior for dislocations in bulk with the same sign.<sup>[11]</sup> Recently, ripples were found to be layer-dependent, which gives rise to an evolving friction behavior in few-layer graphene.<sup>[12,13]</sup> Flexural mode induced ripples add an additional dimension in 2D materials with potential impact on the physical properties.<sup>[14,15]</sup>


## 1. Introduction

The past decade has witnessed the exciting discoveries of 2D materials, which hold interesting electrical, optical and magnetic as well as mechanical properties distinct from bulk. Besides the intrinsic properties featured by monolayer, the stacking of individual monolayers can lead to the observation of numerous exciting physical phenomena.<sup>[1]</sup> For example, Moiré superlattices<sup>[2]</sup> realized by fine control of relative rotational between adjacent 2D layers enabled the discovery of unconventional superconductivity<sup>[3]</sup> and correlated insulating phase<sup>[4]</sup> in magic-angle bilayer graphene, opening up the realization and manipulation of quantum phases via in-plane Moiré engineering. However, 2D materials possess another unique degree of freedom, that is, low-energy flexural out-of-plane bending mode, which becomes more significant with reducing thickness. Such flexibility allows localized stress/strain to be introduced in regions with high curvature which further induce large pseudo-magnetic field and lead to pseudo-Landau levels and quantum Hall effect at high magnetic field regimes that

In parallel, 2D ferroic (e.g., strongly coupled ferroelastic-ferroelectric) and multiferroic<sup>[16–19]</sup> materials recently sparked much interest owing to their potential applications in emerging 2D functional devices. For example, long-range ferromagnetic order was recently discovered in semiconducting CrI<sub>3</sub><sup>[20]</sup> and Cr<sub>2</sub>Ge<sub>2</sub>Te<sub>6</sub><sup>[21]</sup> as well as van der Waals heterostructure<sup>[22]</sup> originating from magnetic anisotropy, which may pave the way for realizing 2D spintronics. Layered transition metal dichalcogenide WTe<sub>2</sub> were found to hold semimetallicity, ferroelectricity,<sup>[23]</sup> and ferroelasticity<sup>[24]</sup> simultaneously, responsible for ferroelectric-switchable nonlinear anomalous Hall effect in few-layer WTe<sub>2</sub> with potential application for nonlinear quantum electronics.<sup>[25,26]</sup> Moreover, van der Waals layered compound In<sub>2</sub>Se<sub>3</sub> was experimentally demonstrated to possess in-plane ferroelectricity,<sup>[27–30]</sup> and group IV monochalcogenides hold strongly coupled ferroelastic-ferroelectric orders with great promise for developing ultrathin memories and actuators.<sup>[31–33]</sup> However, the stability and kinetics of ferroic orders are closely related to the external magnetic, electrical, or stress field, which may be affected by the localized field generated by the intrinsic ripples in 2D materials, suggesting the great importance to understand the role of ripples on 2D ferroicity. Surprisingly, the role of ripples has been largely unexplored in the past, their impact on the physical properties consequently remains largely elusive.

Monolayer group IV monochalcogenides represent a class of strongly coupled ferroelastic-ferroelectric 2D materials with highly anisotropic, strongly coupled, and externally switchable physical properties will engender a wide variety of ultrathin mechano-opto-electronic applications. Among them, GeSe is

Y. Yang, H. Zong, J. Sun, X. Ding  
 State Key Laboratory for Mechanical Behavior of Materials  
 Xi'an Jiaotong University  
 Xi'an 710049, China  
 E-mail: zonghust@xjtu.edu.cn; dingxd@mail.xjtu.edu.cn

 The ORCID identification number(s) for the author(s) of this article can be found under <https://doi.org/10.1002/adma.202103469>.

DOI: 10.1002/adma.202103469

a relatively known case in the aspect of ferroic phase transition.<sup>[32–36]</sup> Herein, we report an atomistic understanding of the effect of ripples on ferroic transformation in monolayer GeSe, including temperature-induced phase transition and stress-induced domain switching. In particular, the ripples increase the relaxation time of high-temperature phase and stabilize the long-range order phase at relatively high temperature. At low temperature, ripples interrupt the long-range interaction among ferroic domains, making the kinetics of domain switching from a collective manner to a random process. Our findings demonstrate that ripples play a crucial role in 2D ferroelasticity and ferroelectricity, and shall be taken into account for 2D materials based device design.

## 2. Results and Discussion

### 2.1. Temperature-Induced Ferroic Phase Transition

Monolayer GeSe belongs to a family of 2D monochalcogenides composed of Group IV and Group VI elements MX, where M = Ge or Sn and X = S, Se, or Te.<sup>[37–39]</sup> Its thermodynamically stable structure is shown in Figure 1a, which exhibits strongly coupled spontaneous polarization ( $\vec{P}$ ) and strain ( $\eta$ ), indicating the coupling between ferroelectricity and ferroelasticity.<sup>[33]</sup> Due to the coupling between ferroelastic and ferroelectric orders, monolayer GeSe has four energetically equivalent domain variants (Figure 1b). We define an atomistic order parameter,  $\vec{R}_p = (\Delta x, \Delta y)$ , to indicate local ferroic orders using the projection of the relative position  $\vec{R} = \vec{R}_{Se} - \vec{R}_{Ge}$  between a pair of Ge and Se atoms onto their local tangent plane. We denote the orientation of the atomistic order parameter  $\vec{R}_p$  by different color, as shown in Figure 1b.

To investigate the effect of ripples on the temperature-induced ferroic phase transition, we first apply a continuous heating-cooling on 2D GeSe from 200 to 400 K. Figure 1c shows the potential energy, which refers to the internal energy of the system due to chemical bonding, as a function of temperature upon heating-cooling cycles. The discontinuity in the potential energy indicates the temperature at which the phase transition occurs, that is,  $\approx 310$  K upon heating and  $\approx 260$  K upon cooling, which shows a weak ramp rate dependency (Figure S1, Supporting Information). The spontaneous strain vanishes in the high temperature phase with the same averaged lattice parameters along  $x$  and  $y$ , resulting in the shape change upon the heating-cooling loop (Figure 1d). Here, we repeated the simulations of heating-cooling loops more than ten times, all of which show similar domain patterns (typical ones in Figure S2, Supporting Information), suggesting the reliability of our molecular dynamics (MD) simulation results. Figure 1e–h shows typical atomistic ferroic orders evolution during the heating-cooling loop. Starting from a single domain 2D GeSe at 200 K with the ferroic orders of  $(\eta_y, -\vec{P}_y)$  as shown in Figure 1e, we heat the sample to 400 K, well above the transition temperature of  $\approx 310$  K. As can be seen in Figure 1f, the long-range ferroic order is absent, while individual “dipole” persists at local atomic sites, sharing the feature of polar nano-regions. The average of the atomistic ferroic orders in the whole sample is zero at high temperature (see Figure S3, Supporting Information). Upon cooling, the long-range order ferroic domains start to nucleate and grow at the temperature of 246 K (Figure 1g), while neighboring domains with different ferroic orders compete with each other. The final structure shows a striped multi-domain pattern when the system is cooling down to 200 K (Figure 1h) which is composed of two energetically equivalent domain variants  $(\eta_y, -\vec{P}_y)$  and  $(\eta_x, -\vec{P}_x)$  separated

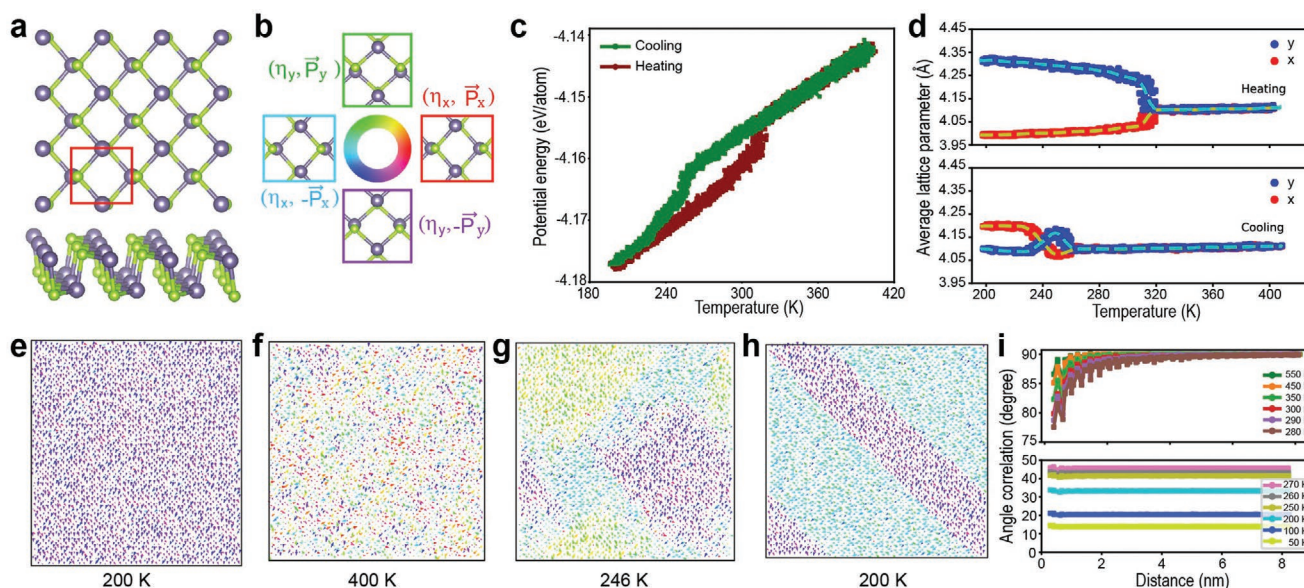


**Figure 1.** Ferroic phase transition in monolayer GeSe. a) Crystal structure of monolayer GeSe. b) Four equivalent domain variants with different spontaneous strain ( $\eta$ ) and polarization ( $\vec{P}$ ). The domains are color coded by the direction of the ferroic orders. c) The evolution of potential energy as a function of temperature upon heating and cooling. d) The average lattice parameters as function of temperature upon heating (upper panel) and cooling (lower panel). e–h) Typical atomic configurations of 2D GeSe at specific temperature upon heating and cooling: e) 200 K, f) 400 K, g) 246 K, and h) 200 K. Each small arrow represents a pair of adjacent Ge–Se atoms. The colors indicate the direction of the Ge–Se dipole, with color map shown in b). i) Temperature-dependent space correlation angle as a function of distance upon cooling.

by two 90° domain walls, consistent with previous experimental observations.<sup>[30,37,40]</sup>

Despite the loss of spontaneous strain in monolayer GeSe at high temperature (400 K), the short-range ferroic order persists in this structure, as shown in Figure 1f. This high-temperature phase is different from the typical bulk para-phase, in which the ferroic orders either disappear or are completely randomized.<sup>[41]</sup> To demonstrate the presence of short-range order in the high-temperature phase, we calculate the space correlation angle  $\theta_{ij}(r)$  at selected temperatures across the transition point, where  $\theta_{ij}(r)$  indicates an average angle between two arbitrary atomistic ferroic order parameters  $\bar{R}_p(i)$  and  $\bar{R}_p(j)$  separated by a finite distance of  $r$ . At each temperature, the structure is equilibrated for 120 ps to generate enough configurations for statistical analysis, and the equilibrium structure upon this cooling can be seen in Figure S4, Supporting Information.  $\theta_{ij}(r)$  at different temperatures upon cooling is shown in Figure 1i. In low-temperature phase,  $\theta_{ij}(r)$  remains constant below 45° over several nanometers, indicating strong angle correlation and long-range ferroic ordering. However, in high-temperature phase,  $\theta_{ij}(r)$  spans between 75° and 90° for  $r < 2$  nm, suggesting the existence of short-range order even above the phase transition temperature. The probability distribution function (PDF) of the angles between two atomistic ferroic orders at specific distance is shown in Figure S5, Supporting Information. The PDFs of high-temperature phase show an obvious change from peaked distribution to random distribution with the increase of distances. All the above results indicate the presence of short-range ferroic order in high-temperature phase. More importantly, ripples may significantly affect the short and long-range ferroic orders in 2D materials, which we will discuss next.

## 2.2. Ripple Effect on Ferroic Phase Transition

To better understand the effect of ripples on the ferroic phase transition, we perform another set of MD simulations in the absence of ripples. In this case, the atoms are only allowed to have in-plane motion, while all the velocities and forces along the out-of-plane direction are fixed at zero. The temperature-dependent magnitude of the atomic ferroic orders is compared with unconstrained models, as shown in Figure 2a. We find that with the presence of ripples the phase transition temperature increases from  $\approx 245$  to  $\approx 275$  K, and the magnitude of the ferroic order is also increased. The increment of mean ferroic order,  $\Delta R$ , shows a linear relationship with temperature except  $T_c$ . This is consistent with the temperature dependence of ripple deformation, which can be represented by the spatially averaged curvature  $\kappa$  (see Experimental Section for the calculation of  $\kappa$ ), as shown in Figure 2c and Figure S6, Supporting Information. Strong correlations between the two quantities are apparent.

Here we calculate  $\frac{1}{N} \sum_N \int (\kappa_i - \bar{\kappa}) (|R_p^i| - |\bar{R}_p|) dt$  to describe the correlation, where  $\kappa_i$  is the curvature at the  $i$ -th Ge–Se pair, and  $|R_p^i|$  is the magnitude of the atomistic ferroic order of the  $i$ -th Ge–Se pair.  $\bar{\kappa}$  and  $|\bar{R}_p|$  are the mean curvature and magnitude of ferroic orders at the given temperature.  $N$  is number of Ge–Se pairs in the structure. The quadratically increased

correlations (Figure 2c) indicate that the ripples at higher temperature can induce stronger local ferroic orders. Besides, we found the thermal fluctuation of ripples can be well described by the well-known thermodynamic model proposed by Gao and Huang,<sup>[42]</sup> that is, the ripple fluctuation of  $h^2$  increases linearly with temperature (Figure 2d).

The ripple deformation also changes the relaxation behavior of 2D ferroic system. Figure 2b compares the temperature-dependent relaxation time  $\tau$  of GeSe under constrained and unconstrained conditions. Here  $\tau$  is estimated from the time auto-correlation function (TCR) of ferroic orders, as shown in Figure S7, Supporting Information. Based on the TCR, we define  $\tau$  as the time delay when the auto-correlation function decays to the inverse of mathematical constant  $e^{-1}$  of its original value at  $t = 0$ . For the low-temperature phase region ( $T \leq 270$  K), the relaxation process is very slow, indicating a relatively static structure. However, a faster relaxation of the ferroic orders is observed in high-temperature phase. As summarized in Figure 2b, the relaxation of the ferroic orders is greatly frozen with the help of ripple deformation. For instance, ripples reduce the relaxation time of  $\tau$  by 23.3% at the temperature of  $2T_c$ .

Besides, the ripple deformation affects the lifetime of local ferroic orders. Figure 2e,g shows the average surface morphology of ripple fluctuations at  $T = 280$  K over a period of 0.2 and 2.0 ps, respectively. We found ripples have cascade structure, and larger ripple fluctuations are longer-lived (Figure 2e,g and Figure S8, Supporting Information). This fluctuation-surviving time relationship is consistent with the ZA mode of phonon dispersions (Figure S9, Supporting Information), agreeing well with previous experimental work, which points out that the ZA mode plays a dominant role in the excitation of ripples.<sup>[43]</sup> The distributions of corresponding atomistic ferroic orders are displayed in Figure 2f,h, respectively. Note that the ferroic orders at the crests and troughs of the ripples possess longer lifetime. This means the ripples can not only affect the overall relaxation time of the ferroic orders, but also extend the lifetime of localized ferroic orders. Ferroic order even remains at some local regions after 100 times  $\tau$  at high temperature due to the presence of relative long-lived ripples (Figure S8, Supporting Information). Ripples therefore can serve as heterogeneous nucleation site upon cooling, thereby promoting the phase transition temperature (see Figure S10 and Video S1, Supporting Information, for the unconstrained model and Figure S11 and Video S2, Supporting Information, for the constrained model). The rippled ferroic phase transition agrees with recent experiments on low-dimensional material, that is, SnTe,<sup>[34]</sup> In<sub>2</sub>Sn<sub>3</sub>,<sup>[30]</sup> and SnS,<sup>[37]</sup> where the co-existence of ripple deformation and ferroic transformation was observed. The present findings suggest that ripple deformation may play an important role in understanding the thickness-dependence of phase transition temperature in SnTe.<sup>[34]</sup>

The results above show a promising method of manipulating ferroic domains in 2D GeSe via tuning ripple fluctuations. Pioneer works have shown the specific ripple fluctuations can be achieved by applying proper compressive strain via substrate engineering,<sup>[44]</sup> strain engineering,<sup>[14]</sup> or using laser patterning.<sup>[45]</sup> Here we investigated the ripple fluctuations as well as the corresponding domain pattern under different biaxial



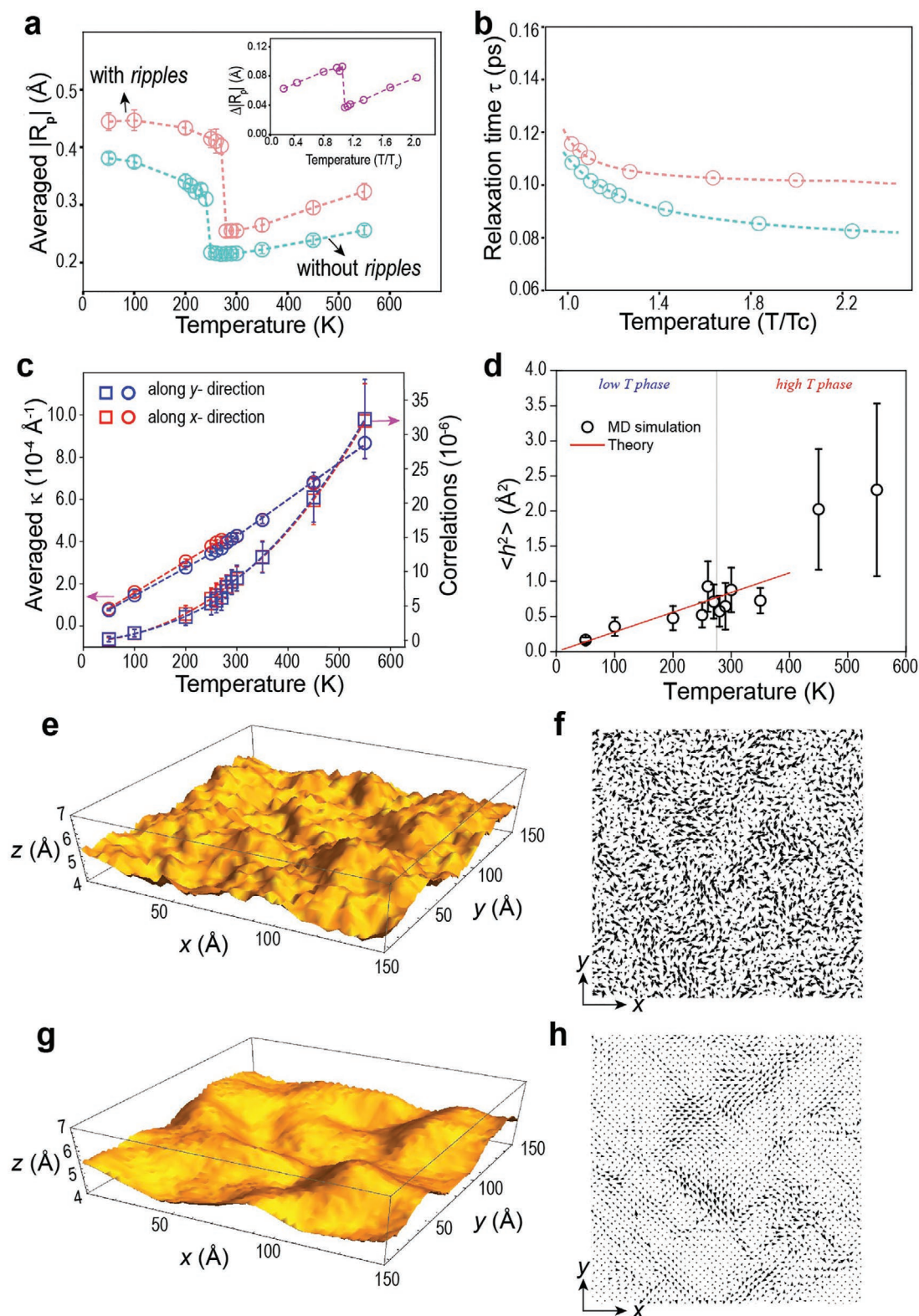


**Figure 2.** The effect of ripples on temperature induced ferroic phase transition in monolayer GeSe. a) The evolution of the averaged magnitude of ferroic orders as function of temperature upon cooling for the unconstrained (pink) and constrained (green) models. b) Temperature-dependent relaxation time  $\tau$  for the unconstrained (pink) and constrained (green) models. c) The evolution of mean curvature  $\kappa$  and the correlations between  $\kappa$  and ferroic orders as function of temperature along x- (red) and y- (blue) directions. d) Comparison of thermodynamic model (solid line) and MD simulations on thermal fluctuations of ripples. e,f) The e) surface morphology and f) local ferroic orders of monolayer GeSe at 280 K averaged over 0.2 ps. g,h) The g) surface morphology and h) local ferroic orders of monolayer GeSe at 280 K over averaged 2.0 ps.

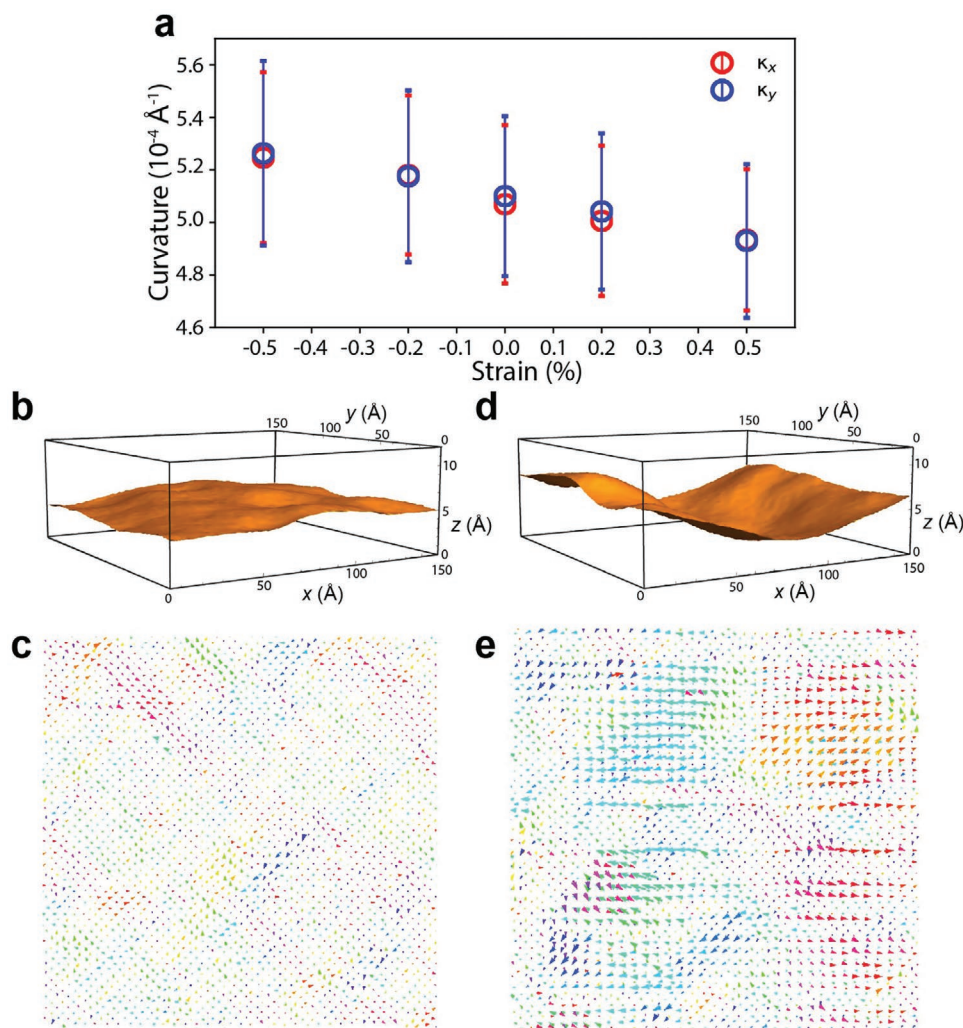


**Figure 3.** Controlling ripple by applying biaxial strain. a) Averaged curvature as function of biaxial strain at 350 K in monolayer GeSe. b,c), The b) surface morphology and c) local ferroic orders of monolayer GeSe averaged over 2.0 ps under 0% strain at 350 K. d,e), The d) surface morphology and e) local ferroic orders averaged over 2.0 ps for monolayer GeSe under 0.2% biaxial compressive strain at 350 K. The ripple deformation is enhanced by compressive strain while relaxed by tensile strain. 0.2% biaxial compressive strain leads to the clear domain patterns (as shown in (d) and (e)). This is different from the stress-free case where no strong ferroic orders are present (as shown in (b) and (c)).

strain (Figure 3a). The ripple deformation is enhanced by compressive strain while eased by tensile strain, and we find the enhanced ripples can give rise to well-developed domain patterns (see Figure 3b–e). Experimentally, such tensile/compressive strain can be engineered into the 2D GeSe via tailoring the pre-strain of the substrates<sup>[46,47]</sup> or the mismatch between monolayers and their substrate.<sup>[48]</sup>

### 2.3. Ripple Effect on Stress Induced Domain Switching

Another interesting aspect is the effect of ripples on the domain switching process, which can help us better understand the multiferroicity in 2D materials. Here, we perform two tensile simulations on monolayer GeSe at 50 K with tensile force applied along  $x$ , that is, one keeps pressure along  $y$  and  $z$  as zero with isothermal-isobaric ensemble (NPT) while the other sets up a biaxial state of stress with canonical

ensemble (NVT). Theoretically, when stretched with NVT ensemble above a critical value, GeSe monolayer can suffer from elastic instability in order to accommodate the in-plane strain incompatibility generated by the Poisson effect, giving rise the formation of ripples.<sup>[49]</sup> This is quite different from the NPT case where the monolayer GeSe only undergoes uniaxial distortion homogeneously, thus not avail to forming ripples.

The stress–strain curve in the NPT case can be divided into three stages, each exhibiting a linear increase of tensile stress followed by a sudden drop where nucleation and growth of new domains take place (blue line in Figure 4a). Initial configuration is shown in Figure 4b, a single domain structure ( $\eta_y, \vec{P}_y$ ) with all atomistic ferroic orders aligned along  $y$ . The first sudden drop at  $\varepsilon = 4\%$  is accompanied by the nucleation and growth of primary twin variants ( $\eta_x, -\vec{P}_x$ ), as shown in Figure 4c,d. The structure remains stable until the second sudden drop at  $\varepsilon = 9\text{--}11\%$ , where secondary twin variants



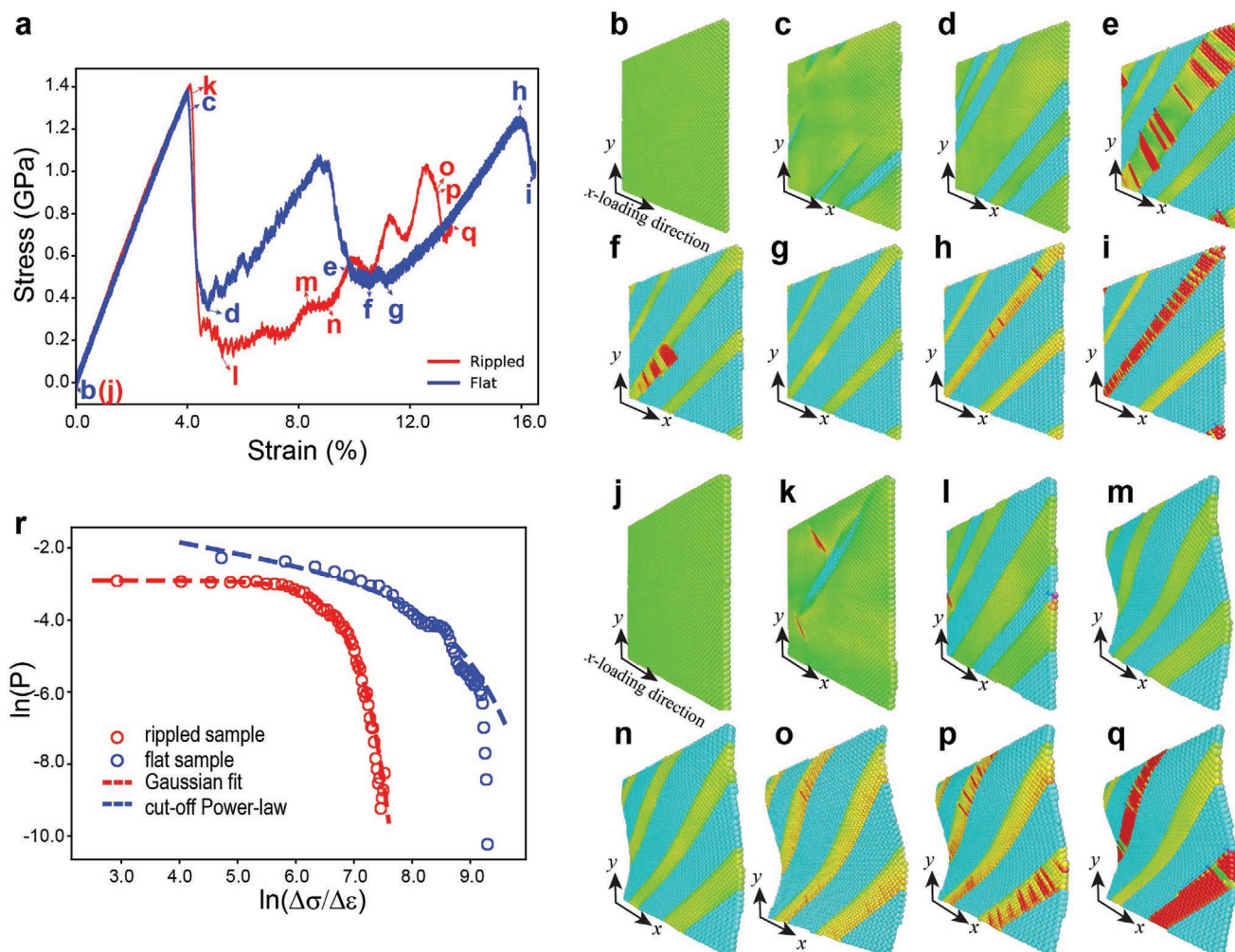


**Figure 4.** The effect of ripples on ferroic domain switching in monolayer GeSe. a) Stress–strain curve in relatively flat (blue) and heavily rippled (red) monolayer GeSe at 50 K. b–i) Typical atomic configurations during stress induced domain switching process in a relatively flat sample. j–q) Typical atomic configurations upon stress induced domain switching in a heavily rippled sample. r) The PDF of stress drop upon tension. Ripples make a cut-off power-law distribution (blue circles) change into a Gaussian distribution (red circles), indicating a transition from collective behavior to ripple-driven random stress relaxation.

$(\eta_x, \vec{P}_x)$  first appear (Figure 4e), then disappear (Figure 4f) due to the competition between the primary and secondary domains. As a result, the primary twin domains grow larger at the end of this stage (Figure 4g). At the third sudden drop at  $\varepsilon = 16\%$ , stable secondary twin domains nucleate and grow (as shown in Figure 4h,i).

In contrast, the NVT simulation shows a quite different mechanical response after the occurrence of ripple deformation. As shown in Figure 4a (red line), the first segment of the stress–strain curve ( $\varepsilon < 4\%$ ) is similar to the first case. The micro-structural evolution involves an elastic deformation followed by the formation of  $90^\circ$  domains (Figure 4j–l). Upon further loading, the variation of the stress is much milder due to the appearance of ripples. These ripples can accommodate the development of domain patterns by changing their curvatures (Figure 4m–q). We note that the nucleation of secondary twin domains appears later than that in the ripple-free case, that is, the nucleation strain of

secondary twin domains in the rippled structure is 12.9% while 9.7% in the ripple-free case. Stress induced ripples can contribute to the tensile deformation, coordinate the lattice distortion, and eventually delay the domain switching process.

We further compare the kinetic behavior of domain switching process, which is quantified by the statistics of the stress drops after the first yielding. Figure 4r shows the PDFs of stress drops in the unrippled (blue) and rippled (red) cases. Without ripple deformation, the PDF of stress drops shows a cut-off power-law distribution. The probability  $P(A)$  is related to the amplitude of the stress drop ( $A \equiv \Delta\sigma/\Delta\varepsilon$ ) as

$$P(A) \sim A^{-\delta} \times \exp\left(-\frac{A}{A_0}\right) \times \left[1 - \exp\left(-\frac{A}{A_1}\right)\right], \text{ where } \delta \text{ equals to } 1.3,$$

and  $A_0$  and  $A_1$  are amplitude thresholds for the power-law distribution. It indicates that there exists highly correlated domain switching dynamics, consistent with previous

observations in 3D ferroelastic materials.<sup>[50]</sup> A typical autocatalytic cascade event is shown in Figure 4e,f, where the growth of the primary twin leading to the disappearance of considerable secondary twins. Differently, we find the dynamics of domain switching in a rippled sample is uncorrelated, as demonstrated by Gaussian distribution of the stress drops. As shown in Figure 4o–q, the secondary twins are formed randomly and their interaction with the primary twins is weakened and localized by the ripples. The NVT and NPT ensembles used in the simulations do not affect the statistical behavior of the domain switching process (see Figure S12, Supporting Information).

### 3. Conclusion

Our present findings demonstrate that ripples add a new degree of freedom for tuning the ferroic properties of 2D materials. On one hand, ripples can release the elastic energy that inevitably appear during the nucleation of ferroic phase, thus influencing the transition temperature and the development of local ferroic order. We note that such effect can even exist at temperature far above the transition point where ripples can stabilize short-ranged ferroic orders. On the other hand, ripples can localize the domain switching process upon loading, and make the evolution of domain patterns from a highly correlated process to a randomly localized process. Our work not only reveals the fundamental role of ripples on 2D ferroicity, but also provides valuable guidance for ripple engineering of controlled phase transition and domain switching in 2D materials with potential applications in 2D flexible electronics.

### 4. Experimental Section

**ML Potential and MD Simulation:** The MD simulations were carried out using the large-scale atomic/molecular massively parallel simulator code<sup>[51]</sup> with an in-house developed machine-learning (ML) potential based on the formulation by Botu and Ramprasad.<sup>[52]</sup> The ML potential was trained with a kernel ridge regression (KRR) based on two assumptions: i) the atomic energy is only related to its local atomic environment, and ii) the total energy of a system is a summation of the energy of all the atoms. The total energy  $E_{tot}$  can be expressed as:

$$E_{tot} = \sum_i E_i = \sum_i \sum_m \alpha_m \cdot K(V_i, V_i) \quad (1)$$

where  $E_i$  stands for the atomic energy of atom  $i$ .  $\alpha_m$  is the  $m$ th-weighting coefficient obtained from the fitting.  $K(V_i, V_i)$  is a linear kernel function as a measure of the distance between the  $i$ th atomic environment features  $V_i$  and the referenced dataset  $V_i$ . The features are physically informed from the nature of structural transformation in 2D materials. In monolayer GeSe, the change of local atomic environment upon phase transition and domain switching can be expressed as a function of covalent bond length and bond angle, which are described by a set of exponentially decayed cosine functions and Gaussian-smoothed radial distribution functions, respectively. A total of 121 features were used to describe the atomic environment (see supplementary A). A large set of configurations were sampled using first-principle molecular dynamic simulations<sup>[53,54]</sup> under different conditions (i.e., different temperature and density) with a  $1 \times 1 \times 1$  k-point grid for a  $4 \times 4$  supercell and then recalculated them with denser k-point mesh of  $3 \times 3 \times 1$ . All the first

principle calculations<sup>[55]</sup> were performed using the Vienna ab initio simulation package<sup>[56]</sup> with the Perdew–Burke–Ernzerhof<sup>[57]</sup> form of exchange–correlation functional within the generalized gradient approximation.<sup>[58]</sup> The kinetic energy cutoff for wave function expansion was fixed to be 300 eV. The GeSe monolayers were modeled in supercells with a vacuum region in the direction perpendicular to the 2D planes of the monolayers (the  $z$  direction). The length of the supercells along the  $z$  direction was chosen to be 20 Å. The energy convergence thresholds for electronic and ionic relaxations were  $10^{-6}$  and  $10^{-5}$  eV, respectively. In the present work, up to 11,893 references were used to train the ML model in order to guarantee the reproducibility of the KRR method (Figure S13, Supporting Information). The properties such as lattice constant, elastic constant, phonon spectrum, phase transition temperature, and transition barrier predicted with our ML potential agree well with density functional theory calculations (see Figures S13–S17 and Table S2, Supporting Information). More details can be found in Supporting Information and <https://github.com/yangymse/GeSe-MLPotential.git>.

Based on the ML force field, the temperature-induced phase transition and stress-induced domain switching in monolayer GeSe were focused on. A supercell with an area of  $40a \times 40b$  was built, where  $a$  and  $b$  are the primitive lattice constants of 3.986 and 4.246 Å at 0 K, respectively. Periodic boundary conditions were applied along the  $x$ - and  $y$ -directions with a free surface along  $z$ . The system was relaxed using isothermal–isobaric ensemble (NPT) at 50 K for 40 ps until equilibrium. Heating and cooling were applied at a rate of 0.77 K/ps. For the structure relaxation at selected temperatures, the magnitude of the ferroic orders, the average curvature, and the space and time correlations were calculated. 4000 configurations over 80 ps were used at each temperature to ensure the validity and precision of the statistical analysis. For tension simulation, a continuous strain rate of  $5 \times 10^8$  per second was applied along  $x$ . This was used in both isothermal–isobaric ensemble (NPT) and canonical ensemble (NVT) simulations. Simulation under isothermal–isobaric ensemble (NPT) yielded a flat monolayer GeSe, while the other yielded the rippled one. Here, the tensile stress was engineering stress, and the effective thickness of monolayer GeSe is defined as the sum of the thickness from top and bottom atoms (2.61 Å) and the van der Waals radii at the top and bottom surface ( $\approx 6.8$  Å). Nosé–Hoover thermostat<sup>[59,60]</sup> was used for temperature control and Parrinello–Rahman barostat<sup>[61]</sup> was used for pressure control.

**Atomistic Ferroic Order Parameter:** There are four equivalent ferroic variants in monolayer GeSe as a combination of spontaneous strain ( $\eta$ ) and polarization ( $\vec{P}$ ):  $(\eta_x, \vec{P}_x)$ ,  $(\eta_x, \vec{P}_y)$ ,  $(\eta_y, -\vec{P}_y)$ , and  $(\eta_y, \vec{P}_y)$ . The ferroic state of these four variants corresponds to the relative displacement of adjacent Ge and Se atoms (Figure 1b). The relative displacement is denoted by vector  $\vec{R} = \vec{R}_{Se} - \vec{R}_{Ge}$ .  $\vec{R}$  is then projected onto the tangent plane of the materials surface to obtain the atomistic ferroic order parameter  $\vec{R}_p = (\Delta x, \Delta y)$ . The  $\vec{R}_p$  was averaged over extensive samplings at a given temperature (i.e., 4000 configurations over 80 ps). The peaked distributions of  $\vec{R}_p$  upon cooling for the unconstrained and constrained models are shown in Figures S18 and S19, respectively, Supporting Information.

**Space Angle Correlations:** Space angle correlations  $\theta_j(r)$  represent the average angle between two ferroic orders separated from a given distance.<sup>[41]</sup>  $\theta_j(r)$  can be calculated as:

$$\hat{D}_i(r_0) \quad (2)$$

where  $\hat{D}_i(r_0)$  is the unit vector of  $\vec{R}_p$  on the  $i$ th Ge–Se pair.  $\hat{D}_j(r_0 + r)$  is the unit vector of  $\vec{R}_p$  on the  $j$ th Ge–Se pair, and the distance between the  $i$ th and  $j$ th pair is  $r$ .  $r_0$  is the position of the  $i$ th Ge–Se pair.  $N$  is the total number of Ge–Se pairs in the system.

**Average Curvature:** Ripple deformation could be described quantitatively by the curvature ( $\kappa$ ) on the monolayer GeSe surface. The curvature around individual atoms could be evaluated as the reciprocal of the radius of its circumscribed circle along specific direction. Herein, two directions,  $x$ -[100] and  $y$ -[010] were chosen to calculate the  $\kappa_x$  and

$\kappa_p$ , respectively. More details can be found in Figure S20, Supporting Information.

**Thermodynamic Model:** The thermal fluctuations of ripples were related to the out-of-plane displacement  $h$ . Then, a classical thermodynamic model proposed by Gao and Huang<sup>[42]</sup> was adapted to derive the thermal fluctuations of ripples as a function of temperature, that is, the mean value of  $h^2$  is expressed as:

$$h^2 \approx \frac{k_B T}{16\pi^3 \delta} S_0 \quad (3)$$

where  $k_B$  is the Boltzmann constant,  $T$  is temperature and  $S_0$  is the initial area of the sample.  $\delta$  is the bending rigidity. For monolayer GeSe, the bending rigidity of low temperature phase is 1.35 eV<sup>[62]</sup> and the initial area of our sample is 27,237.5 Å<sup>2</sup>.

**Time Correlation and Relaxation Time:** First, the time correlation function of atomistic ferroic order parameter  $\bar{R}_p$  was calculated as:

$$\bar{\alpha}_{ij}(t) = \frac{\left[ \frac{1}{N} \sum_i^N \int \bar{R}_p^i(t_0) \bar{R}_p^i(t_0 + t) dt_0 \right]}{\bar{\alpha}_{ij}(0)} \quad (4)$$

where  $\bar{R}_p(t_0)$  is the atomistic ferroic order parameter at  $t_0$ .  $t$  is the time delay, and  $N$  is the total number of Ge–Se pairs in the structure.  $\bar{\alpha}_{ij}(0)$  is a normalize factor to make the time correlation function decay from 1. The relaxation time  $\tau$  is defined as the time delay when the time correlation function decays to the inverse of the mathematical constant  $e^{-1}$ .

## Supporting Information

Supporting Information is available from the Wiley Online Library or from the author.

## Acknowledgements

Y.Y. acknowledges the support by Chinese Scholarship Council (CSC-201706280162).

## Conflict of Interest

The authors declare no conflict of interest.

## Data Availability Statement

The authors declare that all data supporting the findings of this study are included within the paper and its Supplementary Information files. Source data are available from the corresponding authors upon reasonable request.

## Keywords

2D materials, domain switching, ferroic orders, phase transitions, structural defects

Received: May 7, 2021

Revised: September 2, 2021

Published online: October 10, 2021

- [1] K. S. Novoselov, A. Mishchenko, A. Carvalho, A. H. C. Neto, *Science* **2016**, 353, aac9439.
- [2] R. Bistritzer, A. H. MacDonald, *Proc. Natl. Acad. Sci. USA* **2011**, 108, 12233.
- [3] Y. Cao, V. Fatemi, S. Fang, K. Watanabe, T. Taniguchi, E. Kaxiras, P. Jarillo-Herrero, *Nature* **2018**, 556, 43.
- [4] Y. Cao, V. Fatemi, A. Demir, S. Fang, S. L. Tomarken, J. Y. Luo, J. D. Sanchez-Yamagishi, K. Watanabe, T. Taniguchi, E. Kaxiras, *Nature* **2018**, 556, 80.
- [5] F. Guinea, M. I. Katsnelson, A. K. Geim, *Nat. Phys.* **2009**, 6, 30.
- [6] N. Levy, S. A. Burke, K. L. Meaker, M. Panlasigui, A. Zettl, F. Guinea, A. H. C. Neto, M. F. Crommie, *Science* **2010**, 329, 544.
- [7] J. Feng, X. Qian, C. Huang, J. Li, *Nat. Photonics* **2012**, 6, 866.
- [8] H. Li, A. W. Contryman, X. Qian, S. M. Ardakani, Y. J. Gong, X. L. Wang, J. M. Weisse, C. H. Lee, J. H. Zhao, P. M. Ajayan, J. Li, H. C. Manoharan, X. L. Zheng, *Nat. Commun.* **2015**, 6, 7381.
- [9] P. San-Jose, V. Parente, F. Guinea, R. Roldán, E. Prada, *Phys. Rev. X* **2016**, 6, 031046.
- [10] A. Fasolino, J. H. Los, M. I. Katsnelson, *Nat. Mater.* **2007**, 6, 858.
- [11] A. Kushima, X. Qian, P. Zhao, S. Zhang, J. Li, *Nano Lett.* **2015**, 15, 1302.
- [12] C. Lee, Q. Li, W. Kalb, X.-Z. Liu, H. Berger, R. W. Carpick, J. Hone, *Science* **2010**, 328, 76.
- [13] S. Z. Li, Q. Y. Li, R. W. Carpick, P. Gumbsch, X. Z. Liu, X. D. Ding, J. Sun, J. Li, *Nature* **2016**, 539, 541.
- [14] L. Tapasztó, T. Dumitrică, S. J. Kim, P. Nemes-Incze, C. Hwang, L. P. Biró, *Nat. Phys.* **2012**, 8, 739.
- [15] W. Li, X. Qian, J. Li, *Nat. Rev. Mater.* **2021**, 6, 829.
- [16] C. Gong, E. M. Kim, Y. Wang, G. Lee, X. Zhang, *Nat. Commun.* **2019**, 10, 2657.
- [17] Z. Guan, H. Hu, X. Shen, P. Xiang, N. Zhong, J. Chu, C. Duan, *Adv. Electron. Mater.* **2020**, 6, 1900818.
- [18] J. Chu, Y. Wang, X. Wang, K. Hu, G. Rao, C. Gong, C. Wu, H. Hong, X. Wang, K. Liu, C. Gao, J. Xiong, *Adv. Mater.* **2021**, 33, 2004469.
- [19] K. Chang, T. P. Kaloni, H. Lin, A. Bedoya-Pinto, A. K. Pandeya, I. Kostanovskiy, K. Zhao, Y. Zhong, X. Hu, Q.-K. Xue, X. Chen, S.-H. Ji, S. Barraza-Lopez, S. S. P. Parkin, *Adv. Mater.* **2019**, 31, 1804428.
- [20] B. Huang, G. Clark, E. Navarro-Moratalla, D. R. Klein, R. Cheng, K. L. Seyler, D. Zhong, E. Schmidgall, M. A. McGuire, D. H. Cobden, W. Yao, D. Xiao, P. Jarillo-Herrero, X. Xu, *Nature* **2017**, 546, 270.
- [21] C. Gong, L. Li, Z. Li, H. Ji, A. Stern, Y. Xia, T. Cao, W. Bao, C. Wang, Y. Wang, Z. Q. Qiu, R. J. Cava, S. G. Louie, J. Xia, X. Zhang, *Nature* **2017**, 546, 265.
- [22] C. Gong, X. Zhang, *Science* **2019**, 363, eaav4450.
- [23] Z. Fei, W. Zhao, T. A. Palomaki, B. Sun, M. K. Miller, Z. Zhao, J. Yan, X. Xu, D. H. Cobden, *Nature* **2018**, 560, 336.
- [24] W. Li, J. Li, *Nat. Commun.* **2016**, 7, 10843.
- [25] H. Wang, X. Qian, *Sci. Adv.* **2019**, 5, eaav9743.
- [26] H. Wang, X. Qian, *npj Comput. Mater.* **2019**, 5, 119.
- [27] W. Ding, J. Zhu, Z. Wang, Y. Gao, D. Xiao, Y. Gu, Z. Zhang, W. Zhu, *Nat. Commun.* **2017**, 8, 14956.
- [28] Y. Zhou, D. Wu, Y. Zhu, Y. Cho, Q. He, X. Yang, K. Herrera, Z. Chu, Y. Han, M. C. Downer, H. Peng, K. Lai, *Nano Lett.* **2017**, 17, 5508.
- [29] C. Cui, W.-J. Hu, X. Yan, C. Addiego, W. Gao, Y. Wang, X. Wang, L. Li, Y. Cheng, P. Li, X. Zhang, H. N. Alshareef, T. Wu, W. Zhu, X. Pan, L.-J. Li, *Nano Lett.* **2018**, 18, 1253.
- [30] C. Zheng, L. Yu, L. Zhu, J. L. Collins, D. Kim, Y. Lou, C. Xu, M. Li, Z. Wei, Y. Zhang, M. T. Edmonds, S. Li, J. Seidel, Y. Zhu, J. Z. Liu, W.-X. Tang, M. S. Fuhrer, *Sci. Adv.* **2018**, 4, eaar7720.
- [31] M. Mehboudi, A. M. Dorio, W. Zhu, A. van der Zande, H. O. Churchill, A. A. Pacheco-Sanjuan, E. O. Harriss, P. Kumar, S. Barraza-Lopez, *Nano Lett.* **2016**, 16, 1704.
- [32] M. Wu, X. C. Zeng, *Nano Lett.* **2016**, 16, 3236.
- [33] H. Wang, X. Qian, *2D Mater.* **2017**, 4, 015042.



- [34] M. Mehboudi, B. M. Fregoso, Y. Yang, W. Zhu, A. van der Zande, J. Ferrer, L. Bellaiche, P. Kumar, S. Barraza-Lopez, *Phys. Rev. Lett.* **2016**, 117, 246802.
- [35] R. Fei, W. Kang, L. Yang, *Phys. Rev. Lett.* **2016**, 117, 097601.
- [36] R. Fei, W. Li, J. Li, L. Yang, *Appl. Phys. Lett.* **2015**, 107, 173104.
- [37] K. Chang, J. Liu, H. Lin, N. Wang, K. Zhao, A. Zhang, F. Jin, Y. Zhong, X. Hu, W. Duan, *Science* **2016**, 353, 274.
- [38] L. Li, Z. Chen, Y. Hu, X. W. Wang, T. Zhang, W. Chen, Q. B. Wang, *J. Am. Chem. Soc.* **2013**, 135, 1213.
- [39] H. Zhao, Y. Mao, X. Mao, X. Shi, C. Xu, C. Wang, S. Zhang, D. Zhou, *Adv. Funct. Mater.* **2018**, 28, 1704855.
- [40] Y. Bao, P. Song, Y. Liu, Z. Chen, M. Zhu, I. Abdelwahab, J. Su, W. Fu, X. Chi, W. Yu, *Nano Lett.* **2019**, 19, 5109.
- [41] H. Takenaka, I. Grinberg, S. Liu, A. M. Rappe, *Nature* **2017**, 546, 391.
- [42] W. Gao, R. Huang, *J. Mech. Phys. Solids* **2014**, 66, 42.
- [43] J. Hu, G. M. Vanacore, A. Cepellotti, N. Marzari, A. H. Zewail, *Proc. Natl. Acad. Sci. USA* **2016**, 113, 201613818.
- [44] C. H. Lui, L. Liu, K. F. Mak, G. W. Flynn, T. F. Heinz, *Nature* **2009**, 462, 339.
- [45] R. Buividas, M. Mikutis, S. Juodkazis, *Prog. Quantum Electron.* **2014**, 38, 119.
- [46] G. Dong, S. Li, T. Li, H. Wu, T. Nan, X. Wang, H. Liu, Y. Cheng, Y. Zhou, W. Qu, *Adv. Mater.* **2020**, 32, 2004477.
- [47] H. Yuan, K. Wu, J. Zhang, Y. Wang, G. Liu, J. Sun, *Adv. Mater.* **2019**, 31, 1900933.
- [48] S. Zhang, Y. Hou, S. Li, L. Liu, Z. Zhang, X.-Q. Feng, Q. Li, *Proc. Natl. Acad. Sci. USA* **2019**, 116, 24452.
- [49] E. Cerda, K. Ravi-Chandar, L. Mahadevan, *Nature* **2002**, 419, 579.
- [50] E. K. H. Salje, A. Saxena, A. Planes, *Avalanches in Functional Materials and Geophysics*, Springer, New York **2017**.
- [51] S. Plimpton, *J. Comput. Phys.* **1995**, 117, 1.
- [52] V. Botu, R. Ramprasad, *Int. J. Quantum Chem.* **2015**, 115, 1074.
- [53] R. Car, M. Parrinello, *Phys. Rev. Lett.* **1985**, 55, 2471.
- [54] G. Kresse, J. Hafner, *Phys. Rev. B* **1993**, 47, 558.
- [55] W. Kohn, L. J. Sham, *Phys. Rev.* **1965**, 140, A1133.
- [56] G. Kresse, J. Furthmüller, *Phys. Rev. B* **1996**, 54, 11169.
- [57] J. P. Perdew, K. Burke, M. Ernzerhof, *Phys. Rev. Lett.* **1996**, 77, 3865.
- [58] A. D. Becke, *Phys. Rev. A* **1988**, 38, 3098.
- [59] S. Nosé, *J. Chem. Phys.* **1984**, 81, 511.
- [60] W. G. Hoover, *Phys. Rev. A* **1985**, 31, 1695.
- [61] M. Parrinello, A. Rahman, *J. Appl. Phys.* **1981**, 52, 7182.
- [62] S. Kumar, P. Suryanarayana, *arXiv:2003.10936* **2020**.